Semiautomatic vessel wall detection and quantification of wall thickness in computed tomography images of human abdominal aortic aneurysms

Judy Shum
Department of Biomedical Engineering, Carnegie Mellon University, Pittsburgh, Pennsylvania 15213

Elena S. DiMartino[a)]
Department of Biomedical Engineering and Institute for Complex Engineered Systems, Carnegie Mellon University, Pittsburgh, Pennsylvania 15213

Adam Goldhammer
Department of Electrical and Computer Engineering and Department of Biomedical Engineering, Carnegie Mellon University, Pittsburgh, Pennsylvania 15213

Daniel H. Goldman[b)]
Department of Mechanical Engineering and Department of Biomedical Engineering, Carnegie Mellon University, Pittsburgh, Pennsylvania 15213

Leah C. Acker[c)]
Institute for Complex Engineered Systems, Carnegie Mellon University, Pittsburgh, Pennsylvania 15213

Gopal Patel[d)]
Department of Electrical and Computer Engineering and Department of Biomedical Engineering, Carnegie Mellon University, Pittsburgh, Pennsylvania 15213

Julie H. Ng
Department of Mechanical Engineering and Department of Biomedical Engineering, Carnegie Mellon University, Pittsburgh, Pennsylvania 15213

Giampaolo Martufi[e)]
Institute for Complex Engineered Systems, Carnegie Mellon University, Pittsburgh, Pennsylvania 15213

Ender A. Finol[f)]
Department of Biomedical Engineering and Department of Mechanical Engineering, Institute for Complex Engineered Systems, Carnegie Mellon University, Pittsburgh, Pennsylvania 15213

(Received 11 June 2009; revised 16 October 2009; accepted for publication 10 December 2009; published 20 January 2010)

Purpose: Quantitative measurements of wall thickness in human abdominal aortic aneurysms (AAAs) may lead to more accurate methods for the evaluation of their biomechanical environment.
Methods: The authors describe an algorithm for estimating wall thickness in AAAs based on intensity histograms and neural networks involving segmentation of contrast enhanced abdominal computed tomography images. The algorithm was applied to ten ruptured and ten unruptured AAA image data sets. Two vascular surgeons manually segmented the lumen, inner wall, and outer wall of each data set and a reference standard was defined as the average of their segmentations. Reproducibility was determined by comparing the reference standard to lumen contours generated automatically by the algorithm and a commercially available software package. Repeatability was assessed by comparing the lumen, outer wall, and inner wall contours, as well as wall thickness, made by the two surgeons using the algorithm.
Results: There was high correspondence between automatic and manual measurements for the lumen area ($r=0.978$ and $r=0.996$ for ruptured and unruptured aneurysms, respectively) and between vascular surgeons ($r=0.987$ and $r=0.992$ for ruptured and unruptured aneurysms, respectively). The authors' automatic algorithm showed better results when compared to the reference with an average lumen error of 3.69%, which is less than half the error between the commercially available application Simpleware and the reference (7.53%). Wall thickness measurements also showed good agreement between vascular surgeons with average coefficients of variation of 10.59% (ruptured aneurysms) and 13.02% (unruptured aneurysms). Ruptured aneurysms exhibit significantly thicker walls (1.78 ± 0.39 mm) than unruptured ones (1.48 ± 0.22 mm), $p=0.044$.
Conclusions: While further refinement is needed to fully automate the outer wall segmentation algorithm, these preliminary results demonstrate the method's adequate reproducibility and low interobserver variability.
[DOI: 10.1118/1.3284976]

Key words: abdominal aortic aneurysm, computed tomography, wall thickness, automatic segmentation algorithm, biomechanics

I. INTRODUCTION

Abdominal aortic aneurysms (AAAs) are the 13th leading cause of death in the United States[1] and the tenth leading cause of death in white men 65 to 74 years of age, being responsible for at least 15 000 deaths yearly.[2] Most are not detected because AAA disease is largely asymptomatic;[3] the patient exhibits no major symptoms until the aneurysm ruptures. As the abdominal aorta is the largest blood vessel in the body, rupture can lead to heavy internal bleeding. In most cases (30%–50%), the patient dies before he reaches surgery, and even after surgery there is a 50%–70% mortality rate.[4–6] Once an aneurysm is detected, it is repaired or followed up by imaging, depending on the size of the aneurysm at the time of diagnosis. Ultrasound is generally the initial imaging modality in screening programs due to the lack of ionizing radiation, low cost, and portability, but it may not depict the entire abdominal aorta adequately if the patient is obese or if a large amount of bowel gas is present. To clearly define the extent of the disease prior to surgery, the gold standard in imaging is computed tomography angiography (CTA), which is more readily available than magnetic resonance imaging (MRI), and can show the absolute size of the aneurysm and the extent of thrombus present when contrast agent is administered. CTA requires a shorter scanning time than MRI,[7] and is available in a larger number of medical centers. In some cases where the patient's renal function cannot handle the administration of the contrast agent, MRI or magnetic resonance angiography are used as alternatives, but claustrophobia, the patient's inability to remain motionless, and respiratory artifacts can lead to the acquisition of images with poor quality.

Image analysis methods have proven to be invaluable for AAA clinical management.[8] Shape and size information of the aorta is necessary for AAA diagnostics, endovascular procedure planning, and postoperative evaluation. Furthermore, patient specific AAA models have been used successfully to investigate the biomechanics of aneurysms.[9–12] Automatic three-dimensional geometry reconstruction and finite-element mesh generation are necessary tools to bring AAA biomechanics models to the clinics in a timely fashion, compatible with clinical times. Three-dimensional reconstruction to create the AAA biomechanical model requires segmentation of the AAA images. Manual segmentation can also be accomplished; however, it is time consuming and has a low repeatability rate. Thus, an automatic method of segmentation is needed to increase the speed and accuracy of segmentation. The advantages of an automatic image segmentation tool are evident in that not only does it allow one to divide an image into several regions of interest, but it also reduces computation time. Previous works report on vascular lumen segmentation methods.[13] However, segmentation of the outer wall of AAAs is a difficult problem due to the low intensity gradient exhibited by the aortic wall in contrasted images. de Bruijne *et al.*[14–16] used active shape models, while Subasic *et al.*[17] devised a method using a level set, geometric deformable model (GDM). They found that just using the GDM was insufficient as it grew past the boundaries of the aortic wall. To solve this problem, they used varying stopping criteria that would evolve the GDM until the criterion was reached; at that point, another stopping condition was defined.

Vascular biomechanics modeling is highly dependent on the accuracy of the geometric representation of a blood vessel, including a correct representation of the wall thickness.[18] A noninvasive technique for detection of the outer boundary of the vessel wall to quantify the wall thickness of arteries and veins would therefore be valuable in improving the prognostic capabilities of biomechanical models. Furthermore, wall thickness has been shown to correlate with increased degeneration and weakness of the wall;[19] hence, noninvasive detection of wall thickness provides valuable information at the stage of AAA prognosis. A reliable local wall thickness measurement can also be beneficial for producing replicas of blood vessels with variable thickness, as is the case of elastomeric flow phantoms used in bench-top flow visualization experiments.[20] Wall thickness has been measured so far only by invasive methods[19,21] or through MR images of healthy aorta. Hanni *et al.*[22] developed a semiautomatic method of measuring wall thickness in MR images of the rabbit aorta. Adame *et al.*[23] improved on this by developing an algorithm for automatic detection and quantification of wall thickness in MR images of the normal descending aorta. However, their algorithm lacks repeatability among different users, mainly due to blurring between the vessel wall and the surrounding tissue, which makes it difficult to define the contours. Steinman *et al.*[24] measured wall thickness in the carotid artery using a combination of black blood MRI and CFD modeling, but found no clear relationship between hemodynamic variables and wall thickness.

In the present investigation, we present a method to detect and quantify AAA wall thickness using contrast enhanced CT images. This method was recently applied to identify geometric indices we propose to be used in addition to the maximum diameter at the time of AAA diagnosis.[25] We also present an inclusive software suite to perform AAA segmentation and wall thickness detection, which is thoroughly and systematically validated. Moreover, the method is used to study two groups of AAA, ruptured and unruptured aneurysms. It is known that aneurysms undergo many geometrical, histological, and biochemical changes before rupturing (including changes to the wall thickness); therefore, we deemed it important to experiment our methods on these two categories. As such, the objectives of this work are to (i) test the segmentation and wall thickness detection algorithms, (ii) provide an assessment of the reproducibility and interobserver variability of the algorithms, and (iii) assess the accuracy of the software's automatic lumen segmentation and the segmentation provided by commercially available software compared to the reference standard. The outcome of the segmentation tasks can be used by third party image processing software to perform 3D reconstructions of the abdominal aorta. These reconstructions can be further utilized by others to generate computational models suitable for finite element analysis to assess the aneurysm wall mechanics. Moreover, early detection of the changes undergoing in aneurysms be-

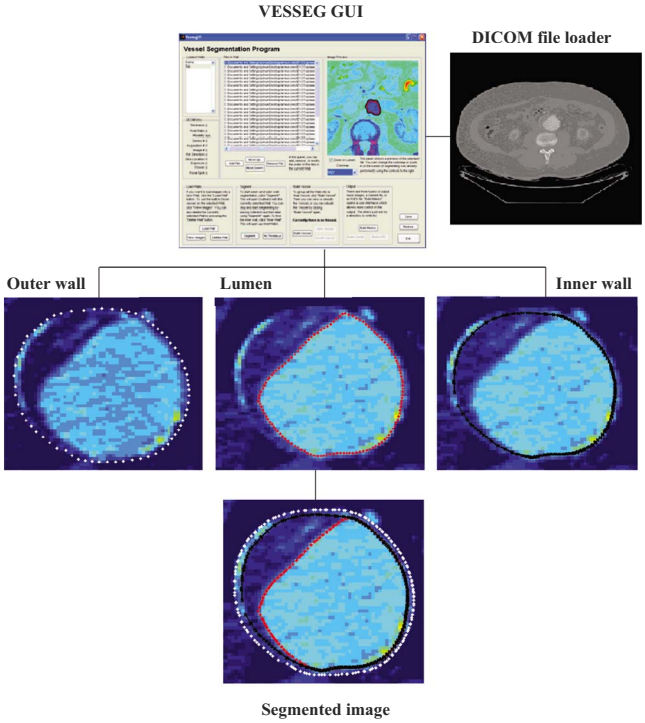

FIG. 1. Schematic of VESSEG interface and segmentation of lumen, outer wall, and inner wall.

fore rupture may help surgeons identify patients at risk of imminent rupture, greatly enhancing the current diagnostic abilities, which are limited to size and rate of growth of AAAs.

II. METHODS

II.A. Subjects and image data

Our study population consists of twenty human subjects with AAAs, ten ruptured ("R" data sets) and ten unruptured ("U" data sets). Noteworthy is that the term "ruptured" is used in the context of this investigation to designate those aneurysms that were detected as ruptured in the last CT exam prior to emergent intervention, as well as those that ruptured within a month after the last CT exam and prior to the intervention. Abdominal DICOM images were acquired using contrast enhanced CT with the following imaging parameters: (i) Scan matrix size=512×512; (ii) pixel size =0.789 mm; (iii) pixel intensity=0–2000; and (iv) slice thickness=2.5 mm (except for U2 and U9 data sets, which were 1.25 and 1.5 mm, respectively).

II.B. Description of the algorithm

The procedure for wall thickness detection involves image segmentation of the lumen, outer wall and inner wall. The DICOM images were imported into an in house MATLAB based image segmentation code (VESSEG v. 1.0.2, Carnegie Mellon University, PA), for the segmentation procedures and wall thickness estimation, as illustrated in Fig. 1. The VESSEG suite of routines was written in MATLAB to provide portability and flexibility to the procedure. A series of specific operations in the VESSEG suite enable segmentation of the lumen and wall of the vessel. Interface with the observer is made possible through a friendly graphical user interface that allows access to all code functions while hiding data structures from the user. Three different algorithms form the basis of the segmentation and wall thickness detection tools applied for the present study and are described below.

II.B.1. Lumen segmentation

The lumen segmentation works best when the CT scanning procedure involves use of a contrast agent since this increases the intensity gradient between the lumen and the surrounding structures. The procedure calls for two simple operations; for the automatic lumen segmentation, the user manually selects only a single sample point inside the lumen and then the routine proceeds to identify the boundary of the lumen by detecting a sufficient gradient for each image in the data set. A gradient image is calculated from the original image and a default threshold level is initialized to determine areas where the gradient image is greater than the threshold. The largest connected region containing the sample point is then labeled as the lumen region. The program verifies the segmentation of every slice subsequent to the first against an average of the previous segmentation and automatically modifies the threshold used for the intensity when needed. In the event that an optimal value for the threshold cannot be found, or if the algorithm detects an incorrect lumen boundary, the user can provide a second threshold by manually selecting a point on the edge of the lumen boundary. The need for a second threshold occurs infrequently (once or twice per data set) and only when the lumen is in close proximity to another region of high intensity, such as the spinal column or wall calcifications, as the segmentation "leaks" into these regions.

II.B.2. Outer wall segmentation

The suite provides two ways of performing outer wall segmentation, manual or automatic. The manual method segments the image by generating an array of contours from which the user chooses the best to represent the outer wall. First, the image is cropped to reduce the image size to areas close to the lumen. A median filter is applied to the image as it reduces the presence of noise and preserves edges. Each output pixel from the filter contains the median value in the 3×3 neighborhood around the corresponding pixel in the cropped image. The median image is then smoothed using an averaging filter of size 3. A contour function is applied that treats the image similar to a topographic map to generate an array of contours or isolines of the image intensity. The user then chooses from the selection of possible contours and, since the contours may not completely surround the lumen, fills in large gaps manually by selecting points along the outer wall. Alternatively, for the automatic segmentation method, the user must enter an intensity threshold by typing it into the graphical interface, which is used to create a boundary that is closest to the lumen without crossing it, and that extends completely around the lumen. Additional control

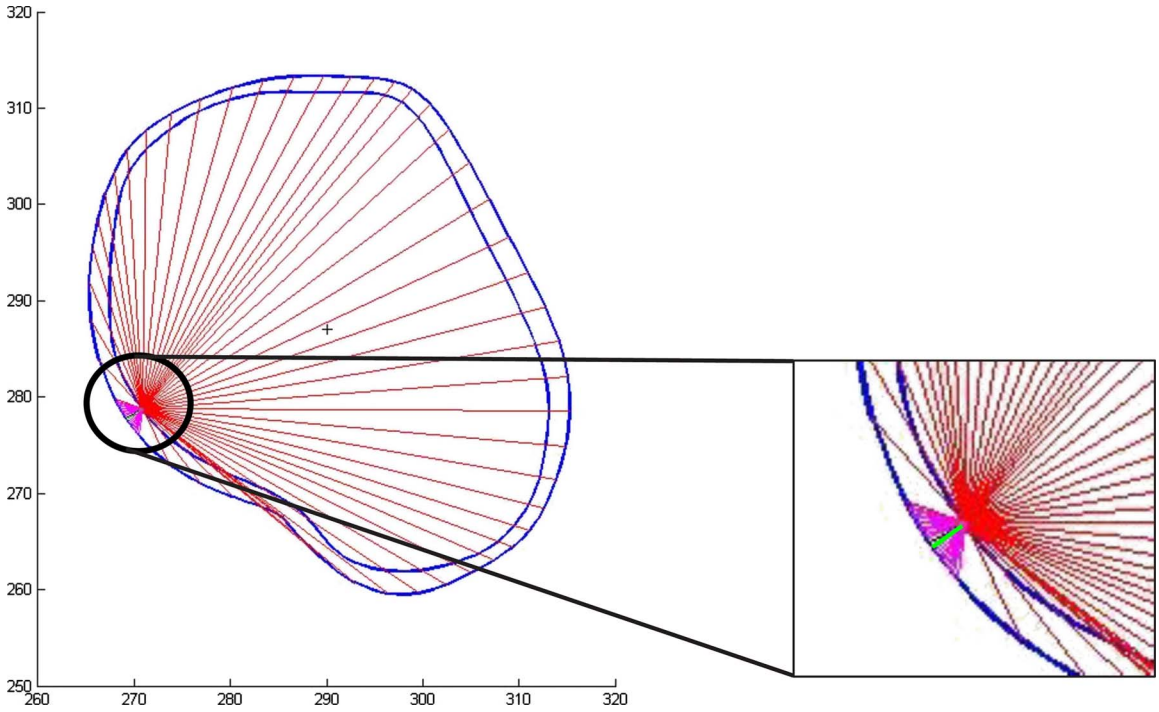

FIG. 2. Visualization of thickness measurement. Radial lines indicate first pass, triangular region second pass, and the perpendicular line shows shortest distance from third pass. Axes units are in pixels, and closed curves represent outer and inner wall contours.

rules embedded in the routine assure that the segmentation of the slice is discarded when possible boundaries are not found; the threshold is then automatically changed to attempt a new segmentation. For those images in which the automatic algorithm cannot detect a contour, the manual method can be used. Additional manual correction is needed for the automatic outer wall algorithm since the pixel intensity of neighboring soft tissues is similar to that of the abdominal aorta, making it challenging to distinguish the boundary of the arterial wall when the two regions are in contact with each other.

II.B.3. Wall thickness detection and quantification

Our algorithm for wall thickness detection is based on the image texture variation across the different structures of the aorta. In brief, flat fielding is used at the outset to enhance contrast in the input image and subsequently the image is processed in parallel by two segmentation algorithms: (a) On one end, a segmentation routine that uses intensity histograms and (b) on the other end, a neural network trained on features of the image set itself. Highlights of our method are the use of a background homogenization function and an *ad hoc* cropping function that reduces the area to be processed to a narrow annular like region around the already segmented lumen region. The neural network is trained by manually extracting samples of background, thrombus and lumen regions, which are used to build the feature vectors necessary for the neural network process. Both intensity based features of the image (mean, standard deviation, and interquartile range), as well as image texture features (such as mean, standard deviation, energy, and homogeneity of the gray level co occurrence matrix) are used by the neural network. The neural network is a single layer with eight nodes, which are texture and intensity based features. The number of elements in the input vector r depends on the number of points the user manually enters during the training. Training stops when the maximum number of epochs is met, in the present application, one thousand. Because of the two-algorithm process carried out on the same duplicated image, two ternary images are created, one obtained from the intensity histogram algorithm and one from the neural network. Both images contain three regions: Background, thrombus, and lumen regions. The neural network produces an "inclusive" thrombus image in that it comprises anything that could be considered thrombus, including the wall. The histogram produces a more conservative thrombus image, only including structures that are definitively thrombus, excluding the wall. Subtracting the two ternary images creates a rough wall image. The process is then refined by inspecting which parts of the rough wall fall in regions of detectable thickness. Only points that are deemed acceptable by the algorithm are included in the wall thickness detection. Finally, smoothing and 3D interpolation algorithms assign wall thickness values to the entire vessel at 72 points (approximately 5° apart) along the inner wall (Fig. 2). Wall thickness is estimated by calculating the distance between a point on the inner wall and its counterpart on the outer wall for which the shortest distance can be calculated. The latter is performed in two steps: First, the algorithm determines a region of interest for a point on the inner wall where the shortest distance exists, as seen in the radial lines in Fig. 2. Next, the distance between the inner wall point and all outer wall points within the region are calcu-

TABLE I. Calculated lumen area for observer 1, observer 2, averaged observers, and automatic method, as well as the relative error between the automatic method and averaged observers for ten ruptured aneurysms.

	R1	R2	R3	R4	R5	R6	R7	R8	R9	R10
Observer 1 (mm^2)	1181.26	1547.61	1668.23	2074.01	1853.99	1806.27	2316.70	885.55	3043.78	1528.75
Observer 2 (mm^2)	1260.68	1553.63	1731.22	2097.89	1959.05	1696.78	2438.82	795.00	3036.48	1390.17
Ave obs (mm^2)	1220.97	1550.62	1699.72	2085.95	1906.52	1751.53	2377.76	840.28	3040.13	1459.46
Automatic (mm^2)	1023.75	1327.49	1753.08	2323.17	2021.21	1680.92	2350.62	730.45	3157.88	1399.44
Relative error (%)	16.93	13.81	−3.38	−11.57	−4.36	3.73	1.15	12.94	−3.51	4.10

lated (triangular region), and the shortest distance (indicated by the perpendicular line) is assigned as the wall thickness.

II.C. Reproducibility and interobserver variability

Statistical analyses of the 20 human AAAs form the statistical population. Each set of CT images was segmented using the proposed method and compared to the reference standard. The latter was defined as the average of the tracings made by two vascular surgeons trained in the use of the segmentation algorithm described in Secs. II B 1 and II B 2. Similar to the statistical methods described in Adame *et al.*,[23] interobserver reproducibility was expressed with standard deviations (SDs) and coefficients of variation (COVs) for calculated wall thickness and lumen, outer wall, and inner wall contours. The reproducibility of the wall thickness, lumen, inner, and outer wall area calculations was assessed on the basis of average areas of two cross sections found in each AAA data set between the renal arteries and the iliac bifurcation. The areas were calculated from the surface area of all the pixels within the region of interest. Bland Altman plots[26] were used, for the lumen region only, to assess the reproducibility between the reference standard and automatic measurements, as well as study the variability between observers.

II.D. Comparison with vascular surgeons' segmentation

We used SCANIP (Simpleware Ltd., Exeter, UK), a commercially available segmentation software, to segment the lumen region of our data sets. A Gaussian filter was applied to all images to smooth any noisy pixels and a region-growing algorithm based on threshold values was used to segment the lumen. Stereolithography representations were made for each model and exported to Rhinoceros (McNeel, Seattle, WA) to compute the lumen areas, which were then compared to those computed using VESSEG. The trained vascular surgeons, with vast experience in CT-based presurgical planning for AAA, were asked to manually segment the lumen area of two cross sections in each data set and the average lumen area was calculated and set as the reference standard. Relative errors were calculated for the lumen area from Simpleware's segmentation and the reference standard, and were compared to the relative error calculated for the lumen area from VESSEG's automatic segmentation and the reference standard.

III. RESULTS

Descriptive statistics for manual measurements made by the vascular surgeons (observers 1 and 2) and the automatic method for lumen segmentation were calculated separately for the ten unruptured and ten ruptured aneurysms (Tables I and II, respectively). The relative lumen area error between the reference standard and the automatic method was, on average, 5.14% (0.60% to 9.58%) for the unruptured and 2.98% (−11.57% to 16.93%) for the ruptured AAA data sets.

III.A. Interobserver variability

Standard deviations and COVs were calculated to determine the degree of interobserver variability between the two observers using the semi automatic algorithm for wall thickness detection, as well as lumen, outer wall, and inner wall segmentations (Table III). The lumen, inner wall, and outer wall contours obtained by the two observers yielded the areas of the three regions for each data set. The average COVs for the lumen area, inner wall area, and outer wall area of the ruptured data sets were 2.77%, 3.01%, and 2.26%, respectively; for the unruptured data sets the average COVs were 2.48%, 3.01%, and 1.94%, respectively.

A linear regression analysis was conducted for each AAA data set to further assess the interobserver variability. Figures

TABLE II. Calculated lumen area for observer 1, observer 2, averaged observers, and automatic method, as well as the relative error between the automatic method and averaged observers for ten unruptured aneurysms.

	U1	U2	U3	U4	U5	U6	U7	U8	U9	U10
Observer 1 (mm^2)	1125.62	836.03	574.20	784.92	1628.63	959.29	494.75	852.34	2008.34	986.40
Observer 2 (mm^2)	1197.12	856.91	590.54	679.77	1656.66	986.11	496.69	881.54	2055.64	1006.28
Ave obs (mm^2)	1161.37	846.47	582.37	732.34	1642.64	972.70	495.72	866.94	2031.99	996.34
Automatic (mm^2)	1061.29	764.45	562.81	729.32	1623.15	924.83	462.80	812.45	1898.20	952.96
Relative error (%)	8.26	9.58	2.98	0.60	1.15	4.85	6.89	6.17	6.60	4.35

TABLE III. Average SD and COV calculated for ruptured and unruptured wall thickness, lumen, inner, and outer wall areas.

	Ruptured				Unruptured			
	Observer 1	Observer 2	SD	COV (%)	Observer 1	Observer 2	SD	COV (%)
Lumen area (mm^2)	1790.62	1795.97	43.93	2.77	1025.05	1040.73	26.60	2.48
Inner wall area (mm^2)	3699.98	3827.09	118.50	3.01	2044.66	1964.29	51.76	3.01
Outer wall area (mm^2)	4333.82	4427.78	103.82	2.26	2311.39	2339.87	39.96	1.94
Wall thickness (mm^2)	2.56	2.34	0.25	10.59	1.55	2.00	0.24	13.02

3(B) and 4(B) show good agreement between the two observers for the lumen area calculation of the ruptured and unruptured aneurysms (r=0.987 and r=0.992, respectively). However, some variability exists, as seen from the Bland Altman plots (Figs. 5(B) and 6(B)), where lumen area measurements made by observer 1 are compared to those made by observer 2 for the ruptured and nonruptured aneurysms, respectively. The average difference between the two observers (15.7 and 5.4 mm^2 for unruptured and ruptured AAAs, respectively) is smaller than that between the reference standard and the automatic method (53.7 and 16.5 mm^2 for unruptured and ruptured AAAs, respectively). Observer 1 had a tendency to underestimate lumen area when compared to observer 2, which can also be seen in the numerical data presented in Tables I and II.

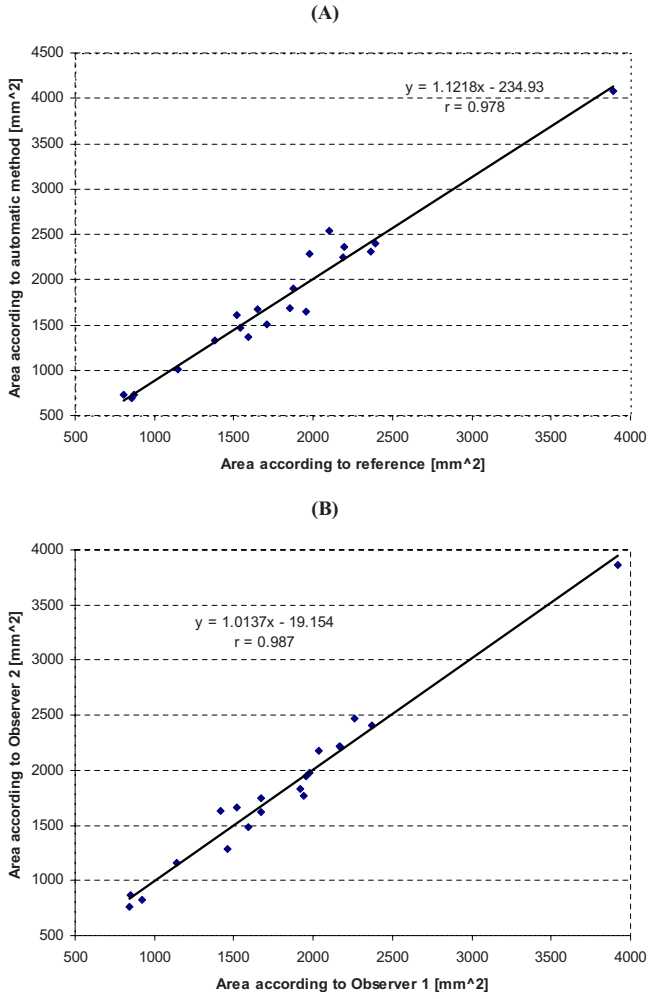

FIG. 3. (A) Linear regression showing the comparison between automatic method and the average contours obtained from both observers, and (B) measurements according to Observers 1 and 2 for lumen area of the ruptured aneurysms.

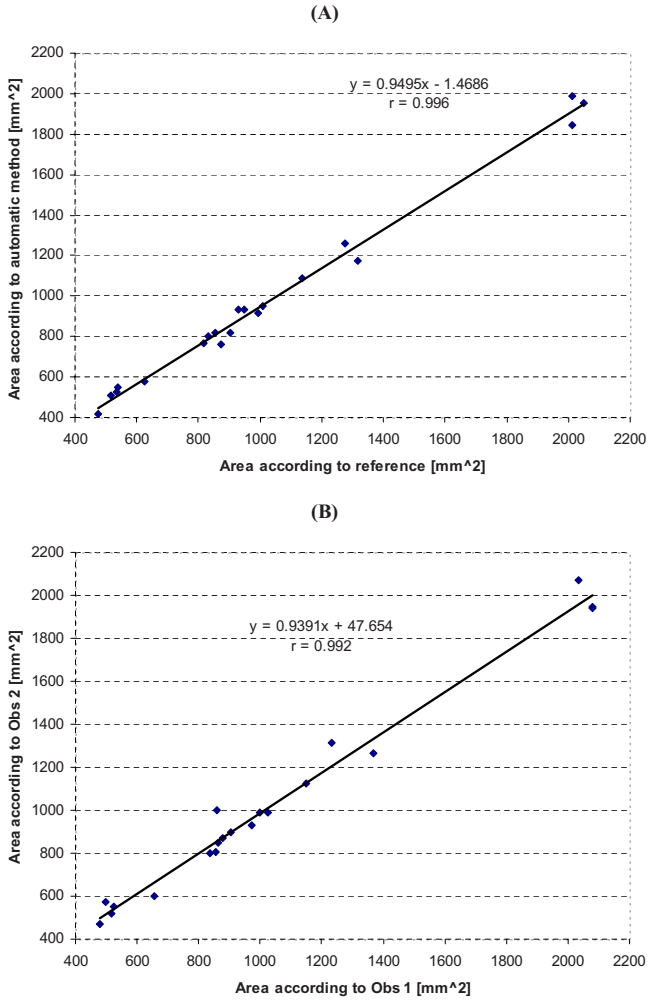

FIG. 4. (A) Linear regression showing the comparison between automatic method and the average contours obtained from both observers, and (B) measurements according to Observers 1 and 2 for lumen area of the unruptured aneurysm.

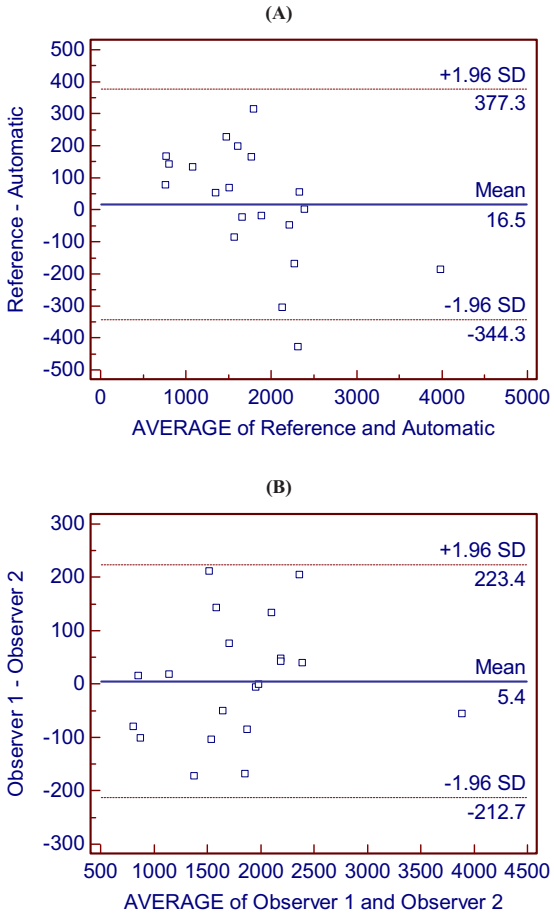

FIG. 5. Bland Altman plot of the differences (A) between automatic and average manual measurements and (B) between Observers 1 and 2, for all ruptured aneurysms.

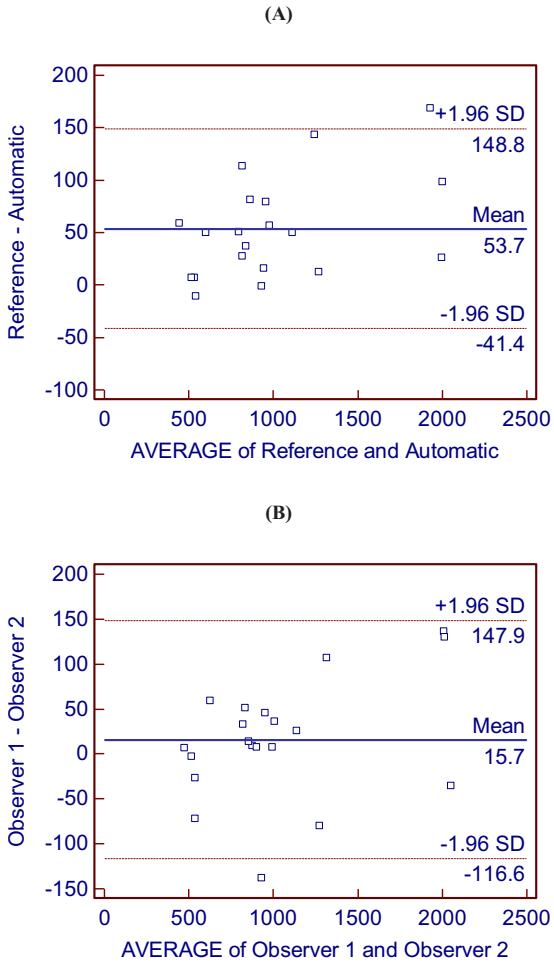

FIG. 6. Bland Altman plot of the differences (A) between automatic and average manual measurements and (B) between Observers 1 and 2, for all unruptured aneurysms.

III.B. Reproducibility

To evaluate how the automatic method compares to the reference standard, Bland Altman [Figs. 5(A) and 6(A)] and linear regression plots [Figs. 3 and 4] illustrate the reproducibility of the automatic and manual lumen area measurements for ruptured and unruptured aneurysms. A high correlation exists for all lumen areas calculated by the observers and the automatic method for all aneurysms [Figs. 3(A) and 4(A)]. From the Bland Altman plots, the automatic method had a tendency to overestimate the lumen area when compared to the reference standard for the ruptured aneurysms [Fig. 5(A)] and to underestimate the lumen area for the unruptured aneurysms [Fig. 6(A)].

III.C. Wall thickness

Average wall thickness, as well as SDs and COVs, were calculated for the ruptured and unruptured aneurysms (Table III). For both data sets, we obtained COVs less than 14% and SDs no greater than 0.24 mm for the unruptured set, and COVs and SDs less than 11% and 0.25 mm, respectively, for the ruptured set. The average ± SD wall thickness of each aneurysm is shown in Table IV. The mean thickness for all the ruptured aneurysms is 1.78 ± 0.39 mm, while for unruptured aneurysms it is 1.48 ± 0.22 mm. Figure 7 illustrates the average wall thickness and standard deviation for each slice in a ruptured aneurysm. The location of the maximum transverse diameter (D_{max}) within the AAA sac is high-

TABLE IV. Average wall thickness (mm) and standard deviation for unruptured and ruptured aneurysms. Mean ± SEM (mm) for each group is shown on the bottom row.

	Wall thickness		Wall thickness
U1	1.39 ± 0.10	R1	2.12 ± 0.14
U2	1.57 ± 0.12	R2	2.12 ± 0.70
U3	1.43 ± 0.14	R3	1.59 ± 0.44
U4	1.41 ± 0.24	R4	1.84 ± 0.48
U5	1.90 ± 0.61	R5	1.48 ± 0.05
U6	1.19 ± 0.08	R6	1.94 ± 0.61
U7	1.34 ± 0.10	R7	1.78 ± 0.68
U8	1.13 ± 0.08	R8	1.76 ± 0.55
U9	1.17 ± 0.23	R9	1.35 ± 0.09
U10	2.25 ± 0.53	R10	1.76 ± 0.21
Mean-unruptured	1.48 ± 0.22	Mean-ruptured	1.78 ± 0.39

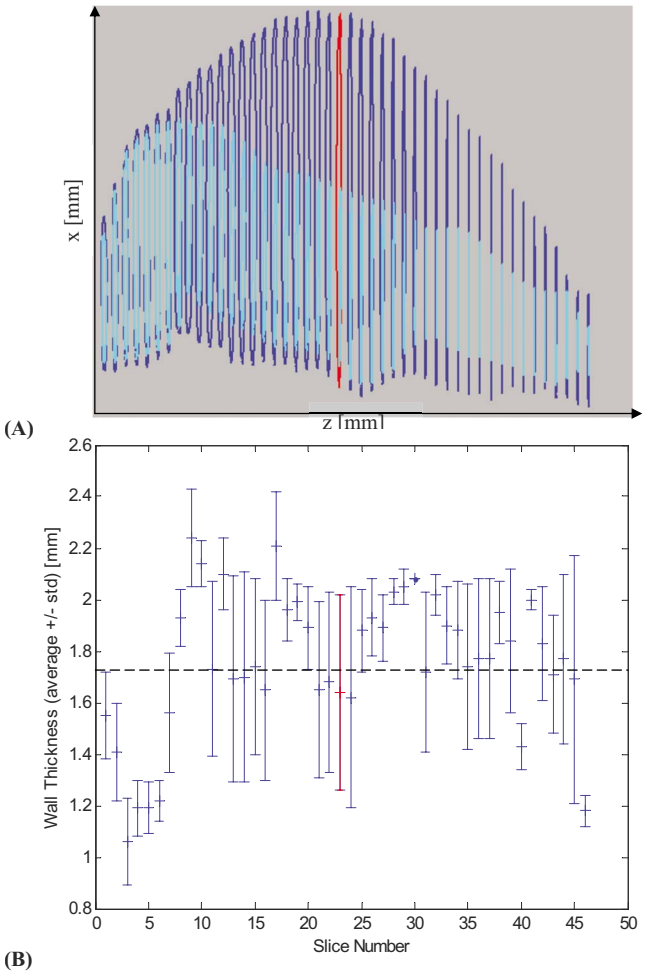

FIG. 7. (A) Lumen and vessel wall contours for each image in the aneurysmal sac (the location of the maximal transverse diameter is highlighted). (B) Average wall thickness and standard of deviation (mm) for a ruptured aneurysm (R10).

lighted. D_{max} is calculated as $D_{max}(i)=4A_i/P_i$, where A_i is the cross sectional area and P_i is the perimeter of the cross section.[24]

III.D. Comparison with commercially available segmentation package

We compared the lumen contours obtained with VESSEG's automatic algorithm and SCANIP, and then compared them to the reference standard. We calculated an average error of 7.53% (range of −28.19% to 65.28%) between SCANIP and the reference standard, and an error of 3.69% (range of −11.57% to 16.93%) between VESSEG and the reference standard. It should be noted that SCANIP does not allow segmentation of the outer wall; no commercial code was found featuring this capability.

IV. DISCUSSION

In this investigation, we report on a method to detect and quantify wall thickness in abdominal aortic aneurysms by segmenting the outer and inner walls of the diseased aorta. The methodology was also recently applied to quantify geometric indices for electively repaired AAA models.[25] Since wall thickness is calculated by measuring the distance from the inner to the outer walls, it is necessary to develop a method that delineates these boundaries accurately. A semi automatic technique for segmenting the lumen, outer wall and inner wall was developed, and statistical analyses were performed to (i) quantify the degree of interobserver variability among tracings made by the two double-blinded observers (trained vascular surgeons) for the lumen, outer wall, and inner wall, and (ii) determine the accuracy of the automatic method in reproducing the lumen tracings made by the observers. Two categories of data sets were considered: Ruptured and unruptured aneurysms. We found that mean wall thickness is larger for ruptured aneurysms. Average interobserver COVs were low for both subject populations in terms of estimation of wall thickness (unruptured=13.02%, ruptured=10.59%) and lumen (unruptured=2.48%, ruptured=2.77%), inner wall (unruptured=3.01%, ruptured =3.01%), and outer wall areas (unruptured=1.94%, ruptured=2.26%). There was good agreement between measurements made by VESSEG's automatic lumen segmentation method and the reference standard with an average relative error of 4.67% for the unruptured and 2.71% for the ruptured data sets.

Previous studies have reported on techniques to measure vascular wall thickness from MR images and using tissue specimens. Adame *et al.*[23] developed an automatic method using a geometric deformable model on *in vivo* MR images of 28 human descending aortas. They report an average wall thickness of 2.0 ± 0.4 mm based on MR images of the healthy aorta in absence of intraluminal thrombus. Wall thickness was also measured by Li *et al.*[27] using four discrete points in the segmented MR images of the healthy thoracic aorta, yielding an average 2.23 ± 0.48 mm. Thubrikar *et al.*[28] measured wall thickness to investigate whether the mechanical properties differ in different regions of the aneurysm. They excised five whole aneurysms with diameters greater than or equal to 5 cm and reported that the posterior region was thicker than the anterior region (2.73 ± 0.46 mm versus 2.09 ± 0.51 mm, respectively). Di Martino *et al.*[19] used a laser micrometer to measure the thickness of AAA wall specimens, obtained fresh from the operating room from patients undergoing surgical repair. A significant difference ($p<0.001$) was found in the wall thickness of ruptured (3.6 ± 0.3 mm) and electively repaired (2.5 ± 0.1 mm) aneurysms, as well as an inverse correlation between wall thickness and local tissue strength. In an autopsy study, Rhagavan *et al.*[18] analyzed the tissue properties of three unruptured and one ruptured AAA revealing that all aneurysms had considerable regional variation in wall thickness and there was a reduction in wall thickness in the vicinity of the rupture site. These two studies differ in that Rhagavan *et al.* measured the thicknesses at the actual site of rupture, whereas Di Martino *et al.* measured thickness of the anterior portion of the aorta, which was not the site of rupture for any of the reported cases. To the best of our knowledge, no other

study has quantified wall thickness of the AAA sac nor has this been measured noninvasively.

The SDs and COVs displayed in Table III for the outer wall and lumen area measurements are comparable to those reported by Adame *et al.*[23] within the context of assessment of interobserver variability. A 3D level set segmentation algorithm developed by Zhuge *et al.*[29] identified lumen and aneurysm areas, in the absence of a method to quantify wall thickness. Their algorithm is limited by the assumption that the shape of the aneurysm is approximately circular in the transaxial cross section, leading to inaccuracies when the aortic cross section is noncircular. Subasic *et al.*[30] also developed a 3D level set algorithm and implemented a deformable model to segment the outer wall and lumen of CTA images. They report an average relative error of 12.35% between lumen segmentations produced by their algorithm and results that were manually corrected.

The automatic method had a tendency to underestimate lumen area when compared to the reference standard (Tables I and II). Since the CT images are contrast enhanced, the lumen appears clearly and is easier to distinguish from the outer wall. However, the intensity is not uniform throughout and large gradients exist within the lumen. Since lumen segmentation is intensity based, the algorithm may detect a gradient within the lumen, which leads to inaccurate delineations of the lumen boundary. As seen in Fig. 8(B), the contours obtained with the automatic method leaves gaps in certain areas, which are not present in the manual segmentations [Figs. 8(C) and 8(D)]. From the linear regression analysis and Bland Altman plots, the automatic method had a tendency to underestimate lumen area when compared to the reference standard for the unruptured aneurysms. This is likely due to the uneven distribution of contrast intensity in the lumen, which causes the algorithm to make a conservative identification of the lumen boundary, leading to smaller area calculations. In addition, the observers' lumen segmentations tend to be smoother than the automatic, as seen in Fig. 8, which would also contribute to the reproducibility discrepancy. The automatic method also showed a slight trend of overestimating lumen area for the ruptured AAAs, as seen in Fig. 5(A). Eleven of the 20 segmented images showed overestimated lumen areas, since the lumen region was harder to distinguish in the ruptured AAAs than the unruptured, likely due to the more evidently inflamed wall in the ruptured aneurysm population.

Native AAAs have complex, tortuous, and asymmetric shapes with local changes in surface curvature[31] and wall thickness. It is evident that an accurate characterization of the aneurysm shape and the regional distribution of wall thickness need to be accounted for in the assessment of AAA biomechanics. The wall thickness measurements show low interobserver variability, as seen in the calculated SDs and COVs. Since wall thickness estimation depends on the outer and inner wall contours, any variability between the contours among observers will also be found in the wall thickness calculations. Moreover, as the average wall thickness of the abdominal aorta is typically in the 1.0–2.0 mm range, the COV defined as SD/average yields undesirably high values

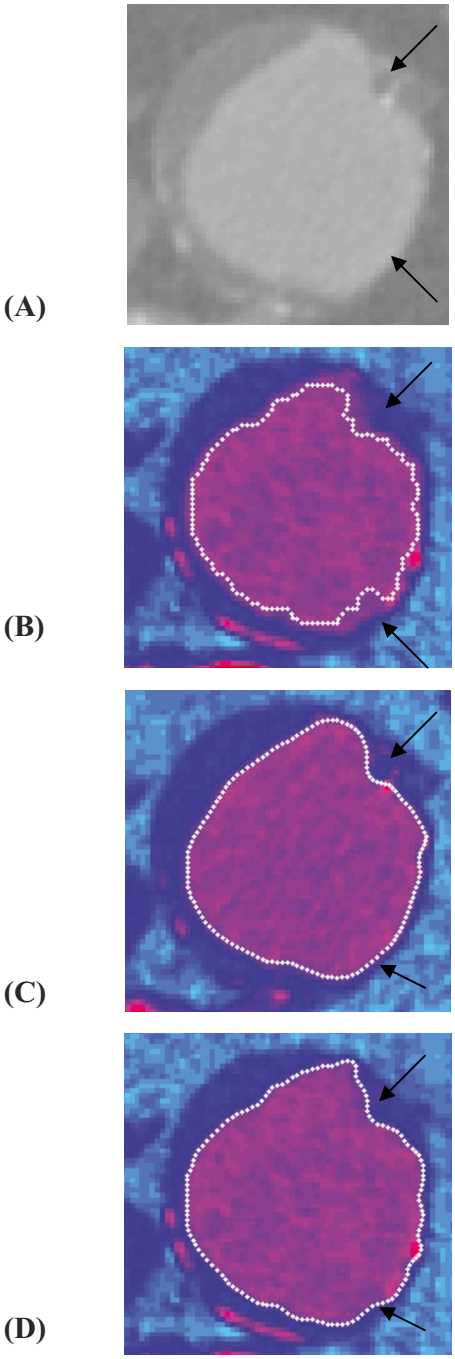

FIG. 8. Lumen contours (white) for an abdominal aortic aneurysm at the midsection of the aneurysm sac. (A) Contrast enhanced CT image; (B) contours drawn using automatic method; (C) contours traced by Observer 1; and (D) contours traced by Observer 2. Arrows point to the part of the contours where the differences between Observers 1 and 2 are more noticeable.

of this statistical measure of interobserver variability. Table IV summarizes the average wall thickness calculated for each aneurysm. Based on two-tailed independent t tests at a significance level of $\alpha=0.05$, we found that the average wall thickness for unruptured aneurysms (1.48 ± 0.22 mm) was significantly smaller ($p=0.044$) than that for ruptured aneurysms (1.78 ± 0.39 mm), which agrees with the results reported by Di Martino *et al.*[19]

The outcome of the present work is subject to important

limitations. While VESSEG is automated to segment the lumen and vessel wall boundaries, user intervention is needed to correct the contours of the outer and inner walls. The automatic lumen segmentation algorithm yields better results than commercial software when compared to the reference standard, with the added caveat that our algorithm is able to segment the vessel wall. However, the outer and inner wall algorithms need to be further refined to yield contours with minimal user intervention. Accuracy and speed can be improved by replacing the 2D lumen segmentation algorithm with a 3D-based algorithm. Zhuge *et al.*[29] implemented a 3D level set algorithm that decreases the computational time it takes to segment the lumen and is able to segment branching structures. They report a mean volume error of $3.5\% \pm 2.5\%$ between their automatic and manual segmentations. Magee *et al.*[32] combined 3D deformable models and level sets and reported that their automatic method was accurate to within two voxels of the interactive method. In addition, segmentation tasks need to include other orthogonal planes of view to yield better results at arterial bifurcations and branches. The number of subjects in the present study is small and there was variability in the slice spacing used to acquire the images. We would also like to explore the use of high resolution MR images with respiratory gating instead of CT. Our algorithm is capable of segmenting both types of images; however, further efforts will be directed to assessing whether MR is a better imaging modality to measure AAA wall thickness given the expected drawback of a lower in-plane resolution.

V. CONCLUSIONS

The method described in this work can be translated into a useful tool for interventional radiologists and vascular surgeons who would need to estimate wall thickness in AAAs for presurgical planning purposes. Having knowledge of regional distributions of wall thickness in native aneurysms can also improve the predictions of biomechanical stresses in a finite element analysis framework. To that end, we described algorithms for lumen and outer wall segmentation, and wall thickness quantification using contrast enhanced abdominal computed tomography images of AAA subjects. We have found that the automatic lumen segmentation method produced better results than commercially available segmentation software when compared to the reference standard. However, to automate wall thickness measurements, additional development is needed to fully automate the outer and inner wall detection algorithms. The lumen segmentation algorithm also requires refinement to lower the interobserver variability and reproducibility of the outcome.

ACKNOWLEDGMENTS

The authors would like to thank Dr. Satish Muluk and the Department of Radiology at Allegheny General Hospital for supplying the CT images used in our study. This work was supported in part by a Bill and Melinda Gates Foundation Millennium Fellowship, the ICES Summer Undergraduate Research Experience (SURE) program, the Pennsylvania Infrastructure Technology Alliance (PITA), and the Biomedical Engineering Department at Carnegie Mellon University.

[a]Present address: University of Calgary, Department of Civil Engineering and Centre for Bioengineering Research and Education, 2500 University Drive NW, Calgary, Alberta, Canada T2N 1N4.
[b]Present address: Neosaej Corporation, 24 New England Executive Park, Suite 105, Burlington, MA 01803, USA.
[c]Present address: Harvard/MIT Division of Health Sciences and Technology, 77 Massachusetts Ave, E25-519, Cambridge, Massachusetts 02139, USA.
[d]Present address: 828 Redgate Road, Dresher, Pennsylvania 19025, USA.
[e]Present address: Royal Institute of Technology, Solid Mechanics, Osquars Backe 1, SE-100 44, Stockholm, Sweden.
[f]Author to whom correspondence should be addressed. Electronic mail: finole@cmu.edu; Telephone: 01.412.268.1841; Fax: 01.412.268.5229.

[1]M. Belkin, M. C. Donaldson, and A. D. Whittemore, "Abdominal aortic aneurysms," Curr. Opin. Cardiol. **9**, 581–590 (1994).
[2]G. R. Upchurch, Jr. and T. A. Schaub, "Abdominal aortic aneurysm," Am. Fam. Physician **73**, 1198–204 (2006).
[3]J. Cornuz, C. Sidoti Pinto, H. Tevaearai, and M. Egger, "Risk factors for asymptomatic abdominal aortic aneurysm: Systematic review and meta analysis of population based screening studies," Eur. J. Public Health **14**, 343–349 (2004).
[4]C. B. Ernst, "Abdominal aortic aneurysm," N. Engl. J. Med. **328**, 1167–1172 (1993).
[5]K. Baskin *et al.*, "Volumetric analysis of abdominal aortic aneurysm," in Proceedings of SPIE Medical Imaging: Physiology and Function from Multi dimensional Images, 1996, Vol. 2709, pp. 323–337 (unpublished).
[6]R. M. Berne and M. N. Levy, in *Cardiovascular Physiology*, 7th ed. (The C.V. Mosby Company, St. Louis, MO, 1997).
[7]J. F. Viles-Gonzalez, M. Poon, J. Sanz, T. Rius, K. Nikolaou, Z. A. Fayad, V. Fuster, and J. J. Badimon, "Multidetector-row computed tomography for the assessment of experimental atherosclerosis: Comparison with magnetic resonance imaging and histopathology," Circulation **110**, 1467–1472 (2004).
[8]J. J. Wever, J. D. Blankensteijn, W. P. Th. M. Mali, and B. C. Eikelboom, "Maximal aneurysm diameter follow-up is inadequate after endovascular abdominal aortic aneurysm repair," Eur. J. Vasc. Endovasc Surg. **20**, 177–82 (2000).
[9]D. A. Vorp, "Biomechanics of abdominal aortic aneurysm," J. Biomech. **40**, 1887–1902 (2007).
[10]M. F. Fillinger, S. P. Marra, M. L. Raghavan, and F. E. Kennedy, "Prediction of rupture risk in abdominal aortic aneurysm during observation: Wall stress versus diameter," J. Vasc. Surg. **37**, 724–732 (2003).
[11]C. M. Scotti, J. Jimenez, S. C. Muluk, and E. A. Finol, "Wall stress and flow dynamics in abdominal aortic aneurysms: Finite element analysis vs. fluid-structure interaction," Comput. Methods Biomech. Biomed. Eng. **11**(3), 301–322 (2008).
[12]J. F. Rodríguez, G. Martufi, M. Doblaré, and E. A. Finol, "The effect of material model formulation in the stress analysis of abdominal aortic aneurysms," Ann. Biomed. Eng. **37**(11), 2218–2221 (2009).
[13]O. Wink, W. J. Niessen, and M. A. Viergever, "Fast delineation and visualization of vessels in 3D angiographic images," IEEE Trans. Med. Imaging **19**, 337–346 (2000).
[14]M. de Bruijne, B. van Ginneken, W. J. Niessen, J. B. A. Maintz, and M. A. Viergever, "Active shape models exploiting slice to slice correlation in segmentation of 3D CTA AAA images," UU CS (Ext. rep. 2001–61) (Utrecht University: Information and Computing Sciences, Utrecht, The Netherlands, 2001).
[15]M. de Bruijne, B. van Ginneken, J. B. A. Maintz, W. J. Niessen, and M. A. Viergever, "Active shape model based segmentation of abdominal aortic aneurysms in CTA images," in *Proceedings of SPIE Medical Imaging*, edited by M. Sonka and J. M. Fitzpatrick (SPIE, Bellingham, 2002), pp. 463–474.
[16]M. de Bruijne, B. van Ginneken, W. J. Niessen, and M. A. Viergever, "Active shape model segmentation using a non linear appearance model: Application to 3D AAA segmentation," UU CS (Ext. rep. 2003–013) (Utrecht University: Information and Computing Sciences, Utrecht, The Netherlands, 2003).
[17]M. Subasic, S. Loncaric, and E. Sorantin, "Model based quantitative AAA image analysis using a priori knowledge," Comput. Methods Programs

Biomed. **80**, 103–114 (2005).
[18]M. L. Raghavan, J. Kratzberg, E. M. Castro de Tolosa, M. M. Hanaoka, P. Walker, and E. S. da Silva, "Regional distribution of wall thickness and failure properties of human abdominal aortic aneurysm," J. Biomech. **39**, 3010–3016 (2006).
[19]E. S. Di Martino, A. Bohra, J. P. Vande Geest, N. Gupta, M. Makaroun, and D. A. Vorp, "Biomechanical properties of ruptured versus electively repaired abdominal aortic aneurysm wall tissue," J. Vasc. Surg. **43**, 570–576 (2006).
[20]J. Seong, C. Sadasivan, M. Onizuka, M. J. Gounis, F. Christian, L. Miskolczi, A. K. Wakhloo, and B. B. Lieber, "Morphology of elastase-induced cerebral aneurysm model in rabbit and rapid prototyping of elastomeric transparent replicas," Biorheology **42**, 345–361 (2005).
[21]A. Nair, B. D. Kuban, E. M. Tuzcu, P. Schoenhagen, S. E. Nissen, and D. G. Vince, "Coronary plaque classification with intravascular ultrasound radiofrequency data analysis," Circulation **106**, 2200–2206 (2002).
[22]M. Hänni, I. Lekka Banos, S. Nilsson, L. Häggroth, and O. Smedby, "Quantification of atherosclerosis by magnetic resonance imaging and 3D morphology operators," Magn. Reson. Imaging **17**, 585–591 (1999).
[23]I. M. Adame, R. J. van der Geest, D. A. Bluemke, J. A. Lima, J. H. Reiber, and B. P. Lelieveldt, "Automatic vessel wall contour detection and quantification of wall thickness in in vivo MR images of the human aorta," Magn. Reson. Imaging **24**, 595–602 (2006).
[24]D. A. Steinman, J. B. Thomas, H. M. Ladak, J. S. Milner, B. K. Rutt, and J. D. Spence, "Reconstruction of carotid bifurcation hemodynamics and wall thickness using computational fluid dynamics and MRI," Magn. Reson. Med. **47**, 149–159 (2002).
[25]G. Martufi, E. S. Di Martino, C. H. Amon, S. C. Muluk, and E. A. Finol, "Three dimensional geometrical characterization of abdominal aortic aneurysms: Image based wall thickness distribution," J. Biomech. Eng. **131**, 061015 (2009).
[26]J. M. Bland and D. G. Altman, "Statistical methods for assessing agreement between two methods of clinical measurement," Lancet **1**, 307–310 (1986).
[27]A. E. Li, I. Kamel, F. Rando, M. Anderson, B. Kumbasar, J. A. C. Lima, and D. A. Bluemke, "Using MRI to assess aortic wall thickness in the multiethnic study of atherosclerosis: Distribution by race, sex, and age," AJR, Am. J. Roentgenol. **182**, 593–597 (2004).
[28]M. J. Thubrikar, M. Labrosse, F. Robicsek, J. Al-Soudi, and B. Fowler, "Mechanical properties of abdominal aortic aneurysm wall," J. Med. Eng. Technol. **25**(4), 133–142 (2001).
[29]F. Zhuge, G. D. Rubin, S. Sun, and S. Napel, "An abdominal aortic aneurysm segmentation method: Level set with region and statistical information," Med. Phys. **33**, 1440–1453 (2006).
[30]M. Subasic, S. Loncaric, and E. Sorantin, "3D image analysis of abdominal aortic aneurysm," Stud. Health Technol. Inform. **77**, 1195–1200 (2000).
[31]M. S. Sacks, D. A. Vorp, M. L. Raghavan, M. P. Federle, and M. W. Webster, "In vivo three-dimensional surface geometry of abdominal aortic aneurysms," Ann. Biomed. Eng. **27**, 469–479 (1999).
[32]D. Magee, A. Bulpitt, and E. Berry, "Combining 3D deformable models and level set methods for the segmentation of abdominal aortic aneurysms," in Proceedings of the British Machine Vision Conference, 2001, pp. 333–341 (unpublished).